APPENDIX

Appendix A. Electroporation Protocol

Before electroporation, one must complete the following:
a) Prepare SOC medium, autoclave.
b) Prepare LB+ agar plates, half with ampicillin and half with kanamycin, autoclave.
c) Clean electroporation cuvettes with 95% EtOH, and rinse them off with DIW thoroughly before use.
d) Autoclave Pasteur pipets, 1 mL pipet tips, 10-200 µL pipet tips, and 1.5 mL epitubes.
e) Chill the chamber slide in the freezer.
f) Bring the rotating incubator up to 37 °C.

1. Thaw electroporation-competent cells on ice. For each sample to be transformed, place two 1.5 mL epitubes and a 0.2 cm electroporation cuvette on ice.
2. In the cold epitube, mix 100 µL of cell suspension with 1 – 2 µL of plasmid DNA in TE buffer. Mix well and incubate on ice for 1 minute.
3. Set up a plastic pipet to deliver 1 mL of SOC medium.
4. Transfer the mixture of cells and DNA to a cold electroporation cuvette and tap or shake the suspension to the bottom. Place the cuvette in the chamber slide and put the slide into to pulser. (See Note)
5. Pulse the cells by holding down both of the pulse buttons simultaneously until it beeps. Quickly remove the chamber slide and immediately add 1 mL of SOC medium and gently resuspend the mixture.
6. Transfer the cell suspension to another sterile 1.5 ml epitube and incubate at 37 °C shaking at 225 RPM for 1 hour.
7. Check and record the pulse parameters.
8. After incubation, plate 1, 10, and 100 µL portions of the SOC suspension onto LB+ agar.

Note: The BioRad E. coli pulser should be turned on and off twice to ensure it is appropriately discharged. Press the "Raise" and "Lower" buttons simultaneously twice to set the voltage to 2.5 kV for the 0.2 cm cuvettes

SOC Medium (100 mL)

Tryptone		2.0 g
Yeast Extract		0.5 g
NaCl	10 mM	0.2 mL from 5 M stock
KCl	2.5 mM	0.25 mL from 1 M stock
$MgCl_2$	10 mM	1.0 mL from 1 M stock
$MgSO_4$	10 mM	1.0 mL from 1 M stock
Dextrose		0.36 g

LB Agar Medium (250 mL)

NaCl	1.25 g
Tryptone	2.5 g
Yeast Extract	1.25 g
Agar	3.75 g

Autoclave the LB agar mixture. When it is cool enough to touch (but before the agar hardens!) add the appropriate antibiotics. It may be useful to make this up in 2 x 125 mL portions if using two antibiotics. Assume 25 mL of broth per plate.

Appendix B. Recipes for Growths and Purifications

15% SDS-Page Gels

15% Resolving Gel	
DIW	2.4 mL
4x stacking gel buffer	2.5 mL
30% acrylamide	5.0 mL
10% APS	150 µL
TEMED	8.0 µL

15% Stacking Gel	
DIW	5.75 mL
4x stacking gel buffer	2.5 mL
30% acrylamide	1.63 mL
10% APS	100 µL
TEMED	12.0 µL

T. maritima D54C/C81S CheY Growth and Purification

Terrific Broth (1 L)	
Tryptone	12 g
Yeast Extract	24 g
KH_2PO_4	2 g
K_2HPO_4	12 g
Glycerol	4 mL

Lysis Buffer, pH 7.5		g/mol	1 L
HEPES	25mM	238.3	5.96 g
NaCl	500mM	58.44	29.22 g
Imidazole	5mM	68.08	0.3404 g
Azide	0.02 %		0.2 g

Wash Buffer, pH 7.5		g/mol	1 L
HEPES	20mM	238.3	4.77 g
NaCl	500mM	58.44	29.22 g
Imidazole	20mM	68.08	1.36 g
Azide	0.02 %		0.2 g

Elute Buffer, pH 7.5		g/mol	1 L
HEPES	25mM	238.3	5.96 g
NaCl	500mM	58.44	29.22 g
Imidazole	200mM	68.08	13.62 g
Azide	0.02 %		0.2 g

10x Thrombin Digestion Buffer, pH 8.0 (1 L)

Tris	500mM	60.75 g
NaCl	1.5mM	87.66 g
$MgCl_2$	50mM	10.17 g
$CaCl_2$	25mM	2.77 g

50 mM Phosphate Buffer, pH 7.2 (1 L)

Prepare 1 M $KHPO_3$

Prepare 1 M KH_2PO_3

Prepare 250 mM EDTA, pH 7.2

Combine 25 ml of 1 M $KHPO_3$, 25 mL of 1 M KH_2PO_3, 4 mL of 250 mM EDTA, and bring to 1 L with DI Water. pH to 7.2 with KOH as necessary.

E. coli D57C CheY Growth and Purification

Lauria Broth (1 L)

NaCl	5 g
Tryptone	10 g
Yeast Extract	5 g

Sonnication Buffer, pH 7.9 at 4 °C (200 mL)

Tris	50 mM	1.21 g
EDTA	1 mM	0.0587 g
PMSF	0.2 mM	0.4 mL from 100 mM stock

30% Sucrose/EDTA Solution, pH 7.5-7.8 (100 mL)

Sucrose	30%	30 g
EDTA	10 mM	0.2922 g

1% Triton/Tris Buffer, pH 7.5 at 22 °C (100 mL)

Tris	50 mM	0.6055 g
EDTA	5 mM	0.1461 g
Triton X-100		1.0 mL

Tris/Urea Buffer, pH 7.5 at 22 °C (100 mL)

Tris	50 mM	0.6055 g
EDTA	1 mM	0.0292 g
Urea	6 M	75 mL of 8 M stock
PMSF	0.2 mM	0.2 mL of 100 mM stock
Azide	0.02%	0.02 g

10x Tris-DEAE Buffer, pH 7.5 at 22 °C (1 L)

Tris	50 mM	6.055 g
EDTA	10 mM	0.2922 g
Azide	0.2%	2.0 g

10x Cibracon Blue Buffer, pH 7.9 (1 L)

Tris	500mM	60.75 g
EDTA	10mM	2.92 g
Azide	0.2 %	2.0 g

2x Dialysis Bag Wash Buffer (500 mL)

$NaHCO_3$	200 mM	8.40 g
EDTA	20 mM	2.92 g

Appendix C. Zip-Tip Protocol

Solution A: 1% Formic acid in water
Solution B: 1% Formic acid in 60% Acetonitrile

Steps 2-6 require depressing and aspirating given solvent 5-10 times
ZipTips: Millipore C18, Tip Size P10, Cat No ZTC18S

1. Evaporate a ~10 µL aliquot of desired sample to dryness and resuspend in 10 µL A
2. Wet Tip with B
3. Equilibrate with A
4. ZipTip sample
5. Rinse sample in A
6. Elute peptides into 3-10 µL B
7. Speed Vac samples to remove B and resuspend in desired solvent or inject on LCMS as such

Notes:

a) ABSOLUTELY DO NOT PIPET AIR THROUGH THE ZIP-TIP.
b) Make up 1 mL of solutions A and B and aliquot them in volumes of 100 µL. This allows for 10 x 10 µL aspirations that are clean and free of contamination.
c) For each sample to be zip-tipped, pipet 10 µL of solution B into a clean 1.5 mL epitube. Aspirate 10 times in this to elute the peptides in step 6.

Appendix D. HPLC Techniques

1. Metal frits are known to bind small amounts of protein that will then not be eluted during normal chromatographic conditions. Passivation of the entire system should be done if variable retention times are seen for some proteins but not all of them. 40 mM EDTA.2Na at a slow flow rate (0.1 mL/min for the 4.6 mmID column) will passivate the frits. Another technique to block frits from interacting with sensitive samples, particularly for new columns, is 2 injections of an inexpensive protein like BSA before any samples of interest.

2. The stationary phase of C-18 columns will slowly degrade if left in the presence of TFA. When the column is to be left overnight or unused for an extended period of time, flush with 5-10 column volumes of a 50% ACN solution with no TFA.

3. The HIC column must be stored in either the low salt buffer or water. It can also be stored in ACN/water (80:20) or in methanol to retard microbial growth. Ammonium Sulfate will precipitate in methanol so be sure to flush both before and after with plenty of water.

4. Standard Operating Conditions:

Column	Flow	Pressure
4.6 x 250 mm C-18 column	1.0 mL/min	100-125 bar
2.1 x 250 mm C-18 column	200 µL/min	100-125 bar
4.6 x 150 mm PolyPropyl A	800 µL/min	100 bar

Apparent retention of standards

Protein	Shallow RP (%, ACN)
Cytochrome *c*	41.3
Lysozyme	43.2 and 44.2
Myoglobin	

5. Troubleshooting

A) The most commonly encountered problems are air bubbles in the pump and sticky check valves (both inlet and outlet). Air bubbles are removed by first making sure the online degasser is on and working. Second, each line should be purged at 5 mL/min with the purge valve open. Sticky check valves must be removed and cleaned. The active inlet valve is a solenoid and should not be cleaned as a whole. Instead, remove the replaceable cartridge and sonnicate in water or methanol. The outlet ball valve can be sonnicated as a whole. If that does not work, the ball itself may be dirty and one should take apart the outlet valve and sonnicate each part individually.

B) Zero dead volume is an easily correctable problem that leads to chromatographic abnormalities such as split peaks and peak broadening. Dead volume is usually created by tubing that is not properly seated at its connection. If you believe the system has dead volume, remove all tubing and reconnect it, making sure all ends are flush before screwing in the fitting.

C) Deuterium lamps have finite lifetimes (usually 1000 hrs). One can check the flowcell parameters on the variable wavelength detector by hitting CTRL + 16. R is the value for pure light and S is the value for the light passing through the flowcell. S should be within 1.5x the value of R but not too much lower. If S is too far off from R, the photocell is dirty and needs cleaning or rebuilding. R should be at least 1 or the lamp needs replacement.

Appendix E. Manuscript Submission to *Biochemistry* (as of 02/23/2007)

The Structures of T87I Phosphono-CheY and T87I/Y106W Phosphono-CheY and Their Binding Affinities to the FliM and CheZ Peptides[†]

Support for this work was provided by the North Carolina Biotechnology Center ARIG Grant Number 9905ARG0026 and by the National Institutes of Health Grant Number 1R15GM063514-01A1. Its contents are solely the responsibility of the authors and do not necessarily represent the official views of the North Carolina Biotechnology Center or the NIH.

Kenneth McAdams[‡], Andrew Mesecar[§,] Bernie Santarsiero[§], Eric S. Casper[‡], R. Matthew Haas[‡], and Christopher J. Halkides[‡*].

‡ Department of Chemistry and Biochemistry, University of North Carolina Wilmington, Wilmington, NC 28403.

[§] Center for Pharmaceutical Biotechnology and Department of Medicinal Chemistry and Pharmacognosy, University of Illinois at Chicago, Chicago, Illinois 60607.

[†] Coordinates and structure factors have been deposited with the Protein Data Bank as entries 2ID7, 2ID9, and 2IDM.

[*] Corresponding Author: Phone (910) 962-7427, Fax (910) 962-3013, Email halkidesc@uncw.edu

Running Title: Structure of Phosphono-CheY Mutants T87I and T87I/Y106W

[1]Abbreviations: CheA, product of the chemotaxis A gene; CheY, product of the chemotaxis Y gene; CheZ, product of the chemotaxis Z gene; CheY~P, phosphorylated form of CheY; EDTA, ethylenediaminetetraacetic acid; DTT, dithiothreitol; DTNB, 5,5'-dithiobis(2-nitrobenzoic acid); FliM, flagellar switch protein M; AMPSO, 3-[(1,1-dimethyl-2-hydroxyethyl)amino]-2-hydroxypropanesulfonic acid; BES, N,N-bis(2-hydroxyethyl)-2-aminoethanesulfonic acid; RP HPLC, reversed phase high-performance liquid chromatography; PEG, polyethylene glycol; MES, 2-morpholinoethanesulfonic acid; Tris, tris(hydroxymethyl)aminomethane; HEPES, N-(2-hydroxyethyl)-piperazine-N'-2-ethanesulfonic acid; RMSD, root mean squared deviation.

Abstract

The structures of T87I phosphono-CheY and T87I/Y106W phosphono-CheY have been solved to 1.8 Å and 1.9 Å. Phosphono-CheY proteins have a phosphonomethyl group on the sulfur atom of D57C variants of CheY, creating an inert mimic of the phosphoryl group attached to Asp57 in the active form of CheY. The increased bulk of I87 forces the side chain of Y106 or W106, a residue known to be critical for signaling, into a more solvent-accessible conformation. Other modest structural changes of the two mutants relative to phosphono-CheY are also observed in the β3-α3 and β4-α4 loops. To correlate the functional changes brought about by the mutations with structural changes of CheY in its active form, the dissociation constants of a peptide derived from the fifteen N-terminal residues of the flagellar motor protein FliM to phosphono-CheY, T87I phosphono-CheY, and T87I/Y106W phosphono-CheY were determined. The FliM peptide binds to phosphono-CheY almost as strongly as it binds to CheY~P. However, this peptide binds T87I phosphono-CheY and T87I/Y106W phosphono-CheY weakly or not at all. Similar results were obtained from a peptide derived from the nineteen C-terminal residues of the phosphatase CheZ to the three variants of phosphono-CheY. One explanation for the failure of the mutants to bind the peptides is that the solvent-accessible rotamer of residue 106 occupies the peptide-binding site. Our results suggest that the known non-signaling phenotype is the result of the mutant proteins' inability to bind downstream targets tightly *in vivo*.

Prokaryotes sense and respond to a variety of environmental signals through the use of two-component systems. In these systems, an autohistidine kinase reversibly transfers a phosphoryl group to a conserved aspartate residue at the active site of the response regulator, controlling its signaling state. CheY is a single domain response regulator that functions in the chemotaxis response (*1*). The histidine kinase CheA transfers a phosphoryl group from its catalytic His residue to Asp57 of CheY, creating CheY~P. CheY~P binds to the switch protein FliM at the base of the flagellar motor and changes its direction of rotation from counterclockwise, generating smooth-swimming behavior, to clockwise, generating tumbly behavior (*2*). The cellular level of CheY~P is reduced by dephosphorylation, through its own autophosphatase activity as well as by the phosphatase CheZ, limiting the *in vivo* half-life of CheY~P to less than a second (*4*). Changes in the concentration of CheY~P determine how frequently the periods of smooth-swimming are punctuated by tumbles; these changes can create a biased-random walk toward a better chemical environment. Mutations in CheY that bring about a greater tendency either toward smooth-swimming or toward tumbly behavior impair chemotaxis (*3*).

A number of structures of *E. coli* CheY in both its activated and inactive states exist in the literature (*5-12*). CheY has $(\beta/\alpha)_5$ saddle topology with its active site near the C-terminus of the central β-sheet. Five highly conserved residues are found near the active site: Asp12, Asp13, Asp57, Thr87, and Lys109. Mutation at any of these conserved residues impairs chemotaxis (*13-16*). The third conserved aspartate, Asp57, is the site of transient phosphorylation (*17*). Figure 1 shows the active-site of phosphono-CheY, in which a cysteine replaces the aspartate residue, and the cysteine residue has been modified with a phosphonomethyl, $-CH_2PO_3$, group to mimic the aspartyl phosphate residue. Mutation of Asp57 produces a protein that cannot be

phosphorylated at the active site and does not bind FliM (*14*, *18*, *19*). Thr87 is involved in the hydrogen bond network at the active site through its γ-hydroxyl group. Certain mutations at residue 87 produce CheY proteins that are phosphorylatable but non-signaling (*15*, *20*). This suggests the importance of residue 87 in propagating conformational changes in the protein upon phosphorylation. T87I CheY is slower in both its autophosphatase activity and its CheZ-promoted phosphatase activity (*15*). The side-chain of Lys109 binds to the phosphoryl group of residue 57 (*10*). Mutant K109R has a similar phenotype to that of T87I CheY (*18*).

Residue 106 is an aromatic residue (tyrosine or phenylalanine) in 80% of known response regulators (*21*). Matsumura and collaborators (*16*) confirmed that an aromatic amino acid at position 106 is required for proper CheY~P signaling. Mutagenesis and structure-function studies indicate that both the identity and the rotameric position of residue 106 are important for CheY~P signaling (*3*, *16*). Substitution of Tyr106 in *E. coli* CheY with tryptophan (Y106W CheY) produces a phosphorylation-dependent hyperactive mutant that generates mainly clockwise rotational bias {Zhu, 1996 #2}. Replacement of Tyr106 with a nonaromatic, nonpolar residue results in completely smooth-swimming cells that are non-chemotactic {Zhu, 1996 #2}.

In crystals of wild-type apo-CheY, Tyr106 is found at the FliM binding surface of CheY (*7*, *22*) and two rotameric conformations are evident from the electron density: an inside, solvent-inaccessible position and an outside, solvent-exposed position. Crystals of Y106W CheY show that tryptophan is found exclusively as the solvent-inaccessible rotamer (*3*). In the structure of T87I CheY, Tyr106 is found only as the solvent-accessible rotamer (*15*). The addition of the ethyl moiety at residue 87 sterically blocks residue 106 from occupying the solvent-inaccessible cavity. Combining these two mutations in T87I/Y106W CheY gives the same phenotype as T87I CheY (*3*), indicating that the T87I mutation is intragenically epistatic to the Y106W

mutation. This result suggests that the buried rotameric conformation of residue 106 is required for CheY~P to induce clockwise rotation of the flagellar motor.

What is the underlying structural basis for the phenotypes of T87I CheY and T87I/Y106W CheY? Does the T87I mutation bring about a defect in binding between CheY~P and FliM or CheZ, or does it cause a post-binding defect? Mutational studies of residue 106 indicated that this residue is not required to bring about affinity between CheY and FliM. Rather, residue 106 is critical in propagating the signal from the active site of CheY~P to FliM to elicit tumbly behavior {Zhu, 1996 #2}. Previous structural studies have examined mutant CheY proteins in their *inactive*, i.e. non-phosphorylated state; however, these studies have generally shown very modest changes between mutant and wild-type structures. This work is the first attempt to explain function with structures in the *active* form.

In this study we describe the changes brought about by phosphonomethylation (to mimic phosphorylation) of T87I CheY and T87I/Y106W CheY and examine whether phosphonomethylation or the T87I mutation controls the rotameric position of residue 106 and the conformation of the loop connecting β4 to α4, the 90s loop. Stable analogues of the phosphorylated states of T87I CheY and T87I/Y106W CheY were prepared similarly to phosphono-CheY (*23*). The structures of these proteins were determined using single-crystal x-ray diffraction. In addition, fluorescence quenching of Trp58 was used to determine the affinities of these two mutants for the FliM and CheZ peptides. The peptide studies allow us to assess whether or not the I87 mutation inhibits binding to FliM or CheZ.

Materials and Methods

Protein Production, Purification, and Modification. *Escherichia coli* D57C/T87I CheY and D57C/T87I/Y106W CheY cloned into separate pet24a(+) plasmid vectors (Novagen) were gifts from Phil Matsumura. Each plasmid was transformed by standard electroporation methods into *E. coli* strain B834 (DE3) (Novagen). Purification of CheY mutant proteins were performed as previously described (*23*) with minor modifications. Cells were lysed with a Fisher 550 sonic dismembrator. Lysozyme to a final concentration of 0.2 mg/mL was occasionally added to assist in breaking the cell walls. In some cases a 2.5 by 54 cm column of Sephadex G-50-150 (Sigma) was used to remove higher molecular weight impurities that remained after the DE52 anion-exchange column and the Affigel Blue (Bio-Rad) column.

Phosphonomethylation of purified D57C CheY variants was performed as previously described (*23*) with minor modifications. Prior to the reaction between CheY and phosphonomethyltriflate, the protein was reduced with 5 mM bis(2-mercaptoethyl)sulfone for up to one hour. CheY protein was exchanged into buffer consisting of 300 mM AMPSO, pH 9.10 with 1 mM EDTA, and strontium chloride or other divalent metal chloride was added to a final concentration of 150-250 mM. An aliquot of ethanol or isopropanol (equal in volume to the volume of triethylamine) was added to phosphonomethyltriflate, then an aliquot of triethylamine consisting of 2.8 moles per mole of phosphonomethyltriflate was mixed in, and this solution was quickly added to the solution of protein with divalent metal ion. The final concentration of phosphonomethyltriflate was 95 to 140 mM. The modification reaction proceeded for 30 minutes, then 10 mM DTT was added. The protein was exchanged into 50 mM BES, pH 7.1 with 2 mM EDTA. At this point the reaction mixture was sampled for RP HPLC and DTNB assays and was roughly 65% complete, though the extent of reaction was variable. Each mixture

of phosphono-CheY and D57C CheY (approximately 250 μM total concentration) was reacted with 2-3 mM PEO-maleimide biotin (Pierce) for 5-12 hrs to attach a biotin group and spacer to unmodified Cys57 residues. Subsequent work has suggested that 2-3 mM PEO-iodoacetyl biotin (Pierce) in 50 mM AMPSO pH 9.0 gives better results (Tyler Davis, unpublished experiments). The mixture of biotinylated D57C CheY and phosphono-CheY was passed over immobilized monomeric avidin (Pierce) to remove biotinylated D57C CheY. Purified phosphono-CheY was concentrated in centricon-3 concentrators (Amicon). T87I phosphono-CheY was also purified from crude reaction mixture by HPLC. A 2.5 x 200 mm ID PolyPropyl Aspartamide anion-exchange column (PolyWax) was equilibrated in the acetate form with 10 CV of 300 mM Na-acetate in 10 mM Tris-acetate, pH 7.0 (mobile phase B) followed by a rinse with 10 CV of 10 mM Tris-acetate, pH 7.0 (mobile phase A). The protein was loaded at 1.0 mL/min in mobile phase A and eluted on a 30 minute gradient of 0-100 % mobile phase B and the effluent monitored at 280 nm. T87I phosphono-CheY eluted approximately 3 minutes after unmodified CheY.

X-ray Crystallography. Crystallization was performed by hanging-drop vapor diffusion. All buffers were filtered through a 0.45 μm membrane except for PEG solutions which were filtered through a glass fiber filter with binder resin, type AP 15 (Millipore). Well solutions were made from 2 M salt, 1 M buffer, and 50% PEG/H_2O stock solutions and mixed on a table mixer for 10 minutes. 1.5 μL of 13-14 mg/mL protein in 5 mM Tris, 0.5 mM EDTA were mixed with 1.5 μL of well solution to form the hanging drop on a silanized cover slip. Small needle-like crystals of T87I phosphono-CheY were grown in 28% PEG 3400, 0.2 M ammonium chloride and 0.1 M sodium acetate, pH 4.60. T87I/Y106W phosphono-CheY crystal 3 was grown in 20% PEG 8000, 0.2 M ammonium acetate and 0.1 M MES-NaOH, pH 5.84. Crystal 4 of T87I/Y106W

phosphono-CheY was grown in 20% PEG 8000, 0.2 M ammonium acetate and 0.1 M MES-NaOH, pH 5.88.

Typically, crystals were soaked briefly in a solution containing all well components in 10% glycerol, frozen in a stream of dry nitrogen, and intensity data collected at 100 K. Data for T87I phosphono-CheY were collected on a Rigaku/MSC R-axis IIc area detector. Data for T87I/Y106W phosphono-CheY were collected on beam line 14BMC at the Advanced Photon Source, Argonne National Laboratory, using an ADSC Quantum-4 detector. Data were processed using the program HKL (*24*).

The structures were solved by molecular replacement with phosphono-CheY (*5*) as the starting model. A test set of 5% of the total reflections were withheld from refinement and used to calculate R_{free}. Iterative rounds of B-factor and positional refinement were carried out with the program CNS (*25*). Toward the end of the refinement cycles, waters were added and a small fraction of the side chains were modeled in two conformations. In one of the structures of T87I/Y106W phosphono-CheY, an acetate ion was included in the final model. The models were validated with the programs Molprobity (*26*), ProCheck (*27*), and What-If (*28*). Table 1 contains crystallographic data and refinement statistics for all three crystals.

Peptide Binding Studies—The binding of the various phosphono-CheY derivatives to peptides derived from FliM and CheZ was studied by fluorescence quenching experiments as previously described (*29*). The FliM peptide consisted of the 16 N-terminal residues of the full-length protein (MGDSILSQAEIDALLN) and the CheZ peptide consisted of C-terminal residues 196-214 (AGVVASQDQVDDLLDSLGF). For fluorescence quenching experiments, peptides were purchased from Global Peptide, Inc. For ITC experiments, peptides were synthesized at the University of North Carolina Microprotein Sequencing and Peptide Synthesis Facility. The

phosphono-CheY samples were titrated with 5 mM and 10 mM stock solutions of the FliM peptide and the CheZ peptide, respectively. Sodium hydroxide to final concentrations of 15 mM and 40 mM were added to the FliM and CheZ peptides, respectively, to obtain a pH of about 7. Solutions of CheY protein were prepared in 5 mM Tris or 50 mM BES, 50 mM NaCl. The peptide and CheY solutions were centrifuged to minimize particulates.

Fluorescence measurements were taken on a Fluoromax spectrofluorometric detector. The experiments were carried out in a 1-mL quartz cuvette containing approximately 2 μM protein in 100 mM HEPES, 10 mM $MgCl_2$, and 0.1% sodium azide. The buffer solution had been filtered through a 0.22 μm syringe filter. The excitation wavelength was 292 nm and the emission wavelength was 345 nm. Slit widths for both excitation and emission wavelengths were 2 nm. A dust-free glass coverslip was used to cover the cuvette during the titration. The temperature was held at 25 °C, and the cuvette was allowed to equilibrate for 6-8 minutes between each addition of peptide.

Fluorescence Data Handling. Corrections were made for the added fluorescence due to the impurities in the peptide. The data were also corrected for dilution of the solution as peptide was added. Fluorescence due to the peptide impurities was first subtracted from the observed fluorescence F_{obs} at a given concentration L_t (total concentration of peptide in the cuvette) according to:

$$F_{corrL} = F_{obs} - f_p * L \qquad (1)$$

where f_p is the fluorescent signal (per unit concentration of peptide) due to the peptide impurities only, which was obtained by titrating the peptide into buffer with no protein. F_{corrL} is the fluorescent signal due to the protein only. The F_{corrL} at each concentration L_t of peptide was then dilution-corrected according to:

$$F_{corr} = F_{corrL} * \frac{(V_o + V_a)}{V_o} \quad (2)$$

where V_o is the initial volume of the solution in the cuvette and V_a is the volume of added peptide stock solution. The corrected fluorescence data were fitted to the hyperbolic ligand-binding function:

$$\Delta F = \frac{L * \Delta F_{\max}}{K_d + L} \quad (3)$$

where ΔF is the difference between the fluorescent intensity with no peptide in solution $\mathbf{F_0}$ and the intensity at a concentration of free peptide **L**. ΔF_{max} is the difference in fluorescent intensity between that at $L_t = 0$ and when all the protein is bound to peptide. K_d is the dissociation constant between the protein and peptide. Since the value of L is the free peptide concentration, and L_t is the sum of the concentrations of free peptide and peptide bound to the protein, L was expressed in terms of the total peptide concentration L_t and the total protein concentration M_t, which are both known quantities (*30*).

$$L = 0.5 * \{L_t - K_d - M_t + \sqrt{(L_t - K_d - M_t)^2 + 4L_t * K_d}\} \quad (4)$$

Additionally, since the protein concentration diminished during the titration, M_t in equation (4) was expressed in terms of the initial protein concentration, M_i, times a dilution correction factor:

$$M_t = M_i * \frac{(C_{pep} - L_0)}{C_{pep}} \quad (5)$$

where C_{pep} is the stock concentration of peptide. The dilution correction factor in equation (5) is equivalent to the reciprocal of the dilution correction factor employed in equation (2). The data consisting of corresponding values of L_t and F_{corr} (with $\Delta F = F_0 - F_{corr}$) were fitted to the composite function of expression (5) into (4), then the result substituted into (3) using

KaleidaGraph (Synergy Software) least squares regression software. No attempt was made to correct for the inner filter effect or nonlinear change of fluorescence of the peptide because the maximum absorbance was kept low enough so that these effects could be ignored without significant errors.

Results

Binding Properties of phosphono-CheY Derivatives. We introduced phosphono-CheY as a non-hydrolyzable (inert) analogue of CheY~P (*23*). Phosphono-CheY is suitable for structural studies which would be difficult for CheY~P (*31*), which has a half-life of 15-20 s even in the absence of CheZ (*32*). The affinities of phosphono-CheY and two other CheY proteins, T87I phosphono-CheY and T87I/Y106W phosphono-CheY, for a FliM-derived peptide and a CheZ-derived peptide were determined by quenching of the fluorescence of W58 (Table 2). Previous work determined the FliM peptide bound CheY~P in a similar manner to intact FliM (*33*), and the CheZ peptide bound about 10 times less strongly to CheY~P when compared to full length CheZ (*29*).

We observe an approximately 17-fold increase in the affinity of the FliM peptide for phosphono-CheY (K_d = 38 ± 1 μM) as compared to that for CheY, slightly higher affinity than what we previously reported (*5*). Compared to phosphono-CheY, CheY~P binds the same FliM peptide with slightly higher affinity (27 ± 1 μM) (*29*). Phosphono-CheY and CheY~P also have similar affinities for the CheZ peptide: CheY~P binds the CheZ peptide about 14-fold more strongly (26 ± 1 μM) than CheY does (*29*), and phosphono-CheY binds the CheZ peptide about 7 times more strongly (58 ± 4 μM) than CheY does. In sharp contrast to phosphono-CheY, T87I phosphono-CheY and T87I/Y106W phosphono-CheY have no measurable affinity for either the FliM or CheZ peptide even upon addition of 500 μM peptide. It is still possible that binding occurs, however, either it is very weak (K_d > 500 μM) or the change in fluorescence is below the level of detection (< 4% of the protein's fluorescence).

Fluorescence quenching was also used to determine the strength of binding of Mg^{2+} to phosphono-CheY, T87I phosphono-CheY, and T87I/Y106W phosphono-CheY. The

dissociation constants are 7 mM, 4 mM, and 7 mM, respectively. The K_d between Mg^{2+} and (unmodified) T87I/D57C CheY is 27 mM. Thus, the phosphonomethyl group brings about a modest increase in the affinity of T87I phosphono-CheY for magnesium ion, relative to a sulfhydryl group.

General Description of Crystallographic Results. All three proteins crystallized in the $P2_12_12_1$ space group with 1 molecule per asymmetric unit. The final model of T87I phosphono-CheY refined to 1.75 Å contains 128 residues with 983 atoms and 116 water molecules. Crystal 3 of T87I/Y106W phosphono-CheY refined to 1.85 Å contains 128 residues with 985 atoms and 79 water molecules. Crystal 4 of T87I/Y106W phosphono-CheY refined to 2.00 Å contains 128 residues with 986 atoms, 100 water molecules, and 4 acetate atoms. The structures refined with good chemical geometries. The Ramachandran plots showed that all residues fell within the allowed region, except for Asn62, the central residue of the γ-turn (*21*). Structural statistics and refinement data are given in Table 1 andadditional refinement statistics are included in the supplemental material.

Overall Comparison of T87I CheY with T87I phosphono-CheY. The overall changes upon phosphonomethylation are rather modest. Superposition of Cα coordinates of T87I phosphono-CheY with molecules A and B of T87I CheY yields root mean square deviations of 0.55 Å and 0.49 Å, respectively, slightly higher than the RMSD of 0.38 Å observed *between* T87I CheY molecules A and B (*15*). The side-chains of 4 glutamate and 3 lysine residues are found in multiple conformations, but these are all solvent exposed side-chains. Additionally, Phe14 is found *cis* to its amide nitrogen (g+), whereas it is g- in T87I CheY. Phe14 may have importance in the binding of the P2 domain of CheA (*34*) and CheZ (*35*).

δ-distance mapping (Figure 1 in supplemental material) indicates that residues 88-94 shift towards the active site upon phosphonomethylation, consistent with the changes observed in the structure of BeF_3•CheY relative to apoCheY. When the Cα atoms of residues least affected by modification of T87I CheY (residues 10-86) are superposed, it is evident that the most significant differences occur in the 90's loop between β–strand 4 and helix 4 (Figure 4a in supplemental material).Lys91 shows the greatest displacement (2.0 Å) between corresponding Cα atoms. In T87I phosphono-CheY there is a second hydrogen bond between Glu89 Oε and Lys91 Nε in addition to the hydrogen bonding already described for T87I CheY between the backbone carbonyl of Glu89 and backbone amide of Lys91 (*15*). It is not known whether or not this hydrogen bond is present in T87I CheY since the side chain atoms of Glu89 and Lys91 in T87I CheY had poor electron density. The positions of the atoms in the 90's loop in T87I CheY and T87I phosphono-CheY structures differ by greater than 1.5 Å, demonstrating the flexibility of the loop (Figure 2). We cannot exclude that crystallization conditions or packing forces contribute to the differences seen in the two structures since intermolecular contacts involving residues 91-98 are present in T87I CheY (*15*), and we observe a crystal contact involving the backbone amide of Ala90. T87I CheY crystallizes in space group $P2_1$ with two molecules per asymmetric unit.

The other significant difference in the T87I phosphono CheY structure when compared to T87I CheY is the displacement of α-helix 5 away from the active site. This can be visualized as a downward shift of the helix ~0.8 Å parallel to its helical axis and is supported both by Cα superposition and δ-distance mapping (see supplemental material) This is comparable in magnitude but in the opposite direction to that seen in BeF_3•CheY (*10*).

Structure at the Active Site of T87I phosphono-CheY. In the structure of T87I phosphono-CheY, two distinct regions of electron density define the position of the phosphonomethyl moiety (Figure 3). We refer to these rotamers as Pcy57 A and B. Pcy57 A resembles T87I/Y106W phosphono-CheY (see below) and is intermediate between the positions of Pcy57 B and the phosphonomethyl group in phosphono-CheY (*5*). A phosphoryl oxygen in Pcy57 A is 2.8 Å from Lys109 Nε but is ~ 4 Å from the backbone amides of Trp58, Asn59, and Ala88 (Table 3). Pcy57 B is close to Asn59 (2.7 Å from PO_3 to Asn59 NH), however it is ~ 3.5 Å from Lys109 Nε and the backbone amides of Trp58 and Ala88. Ile87 is positioned ~0.5 Å closer to the phosphoryl group despite lacking the hydroxyl group involved in the hydrogen bond network at the active site in BeF_3•CheY; however, the two residues are not in contact. A solvent molecule defined as water82 interacts with Asn59 CO, Asp13 Oδ, a phosphoryl oxygen, and up to three other side-chains or water molecules. It is similar to water molecules observed in the apo-CheY structure (*11*) and the CheY•CheZ peptide structure (*4*), neither of which have a divalent metal ion. It is possible that the presence of a divalent metal ion would result in less variation in the position of the phosphomethyl group than is observed in T87I phosphono-CheY.

Overall Comparison of T87I/Y106W CheY with T87I/Y106W phosphono-CheY. X-ray diffraction data from two crystals of T87I/Y106W phosphono-CheY gave nearly identical structures (RMSD ~0.25 Å), which we call crystals 3 and 4 (Supplemental Material). The overall RMSD of Cα coordinates of this structure compared with T87I/Y106W CheY is 0.46 Å and 0.49 Å for crystal 3, which is similar to the Cα RMSD between residues 2-86 of the two molecules A and B of T87I/Y106W CheY (0.42 Å) (*3*). Side-chain conformations in the core of the molecule are very similar in T87I/Y106W phosphono-CheY and T87I/Y106W CheY, but variations are seen in the charged, solvent-exposed residues. Phosphonomethylation does not

bring about large-scale conformational changes in T87I/Y106W CheY, but it does cause changes in the 60's loop (residues 59-64) and the 90's loop (residues 88-91).

The δ-distance plot comparing T87I/Y106W phosphono-CheY with T87I/Y106W CheY indicates the loop around residue 60 moves ~1 Å away from helix 2 upon phosphonomethylation, a result of a 39° rotation about dihedral angle ψ of residue 57 (Figure 3 in supplemental material). The superposition of Cα coordinates of the entire structures of T87I/Y106W CheY with T87I/Y106W phosphono-CheY indicates the Cα atoms of Pcy57 and Asp57 are essentially identical (0.3 Å), but the Cα atoms of Trp58 and Asn59 differ by 0.8 Å and 1.1 Å, respectively. A superposition using the residues least affected by modification (5-50) magnifies the differences in the Cα atoms of Trp58 and Asn59 to 0.9 Å and 1.4 Å, respectively (Figure 4 in supplemental material). The conformations of side-chains of residues in the β3-H3 loop remain essentially the same, so the displacement of the main chain may or may not have functional significance.

A change is also observed in the 90's loop, albeit to a lesser extent than what is observed with T87I phosphono-CheY (Figure 2). The pseudodihedral angle defined by the Cα atoms of residues 87 through 90 does not change appreciably upon phosphonomethylation (Table 4). Despite this fact, the Cα atom of Ala88 is 1.0 Å further from β5 in T87I/Y106W phosphono-CheY than T87I/Y106W CheY, a result of the 53° rotation about dihedral angle ψ of Ala88. Slightly smaller changes are observed for the two flanking residues; however, residues 90-94 remain essentially unchanged, unlike what is seen in T87I phosphono-CheY. Overall, phosphonomethylation produces similar conformational changes for the T87I/Y106W mutant as it does for the T87I mutant. The δ-distance plots (supplemental material) of T87I/Y106W phosphono-CheY versus T87I/Y106W CheY compared with T87I phosphono-CheY versus T87I

CheY reveal that the 60's loop moves further away from helix 2 upon phosphonomethylation, but the 90's loop does not move away from helix 5.

Structure at the Active Site of T87I/Y106W phosphono-CheY. The phosphoryl groups in the two structures of T87I/Y106W phosphono-CheY are found in nearly identical positions; however, this position is distinct relative to the same group in phosphono-CheY and T87I phosphono-CheY (Figure 4). The hydrogen bonds between oxygen atoms of the phosphoryl group and Trp58 NH, Asn59 NH, Ala88 NH, and Lys109 Nε implied by the structure of BeF_3•CheY (*10*) appear to be longer in T87I/Y106W phosphono-CheY (Table 3). It is noteworthy that the phosphoryl group in T87I/Y106W phosphono-CheY crystallizes in a position more similar to that of BeF_3 than in any of the other phosphono-CheY proteins.

Position of Residue 106 in the two mutants. A necessary part of the activation of CheY-like response regulators is the rotation of residue 106 from the g- (solvent-accessible conformer) to a g+ (solvent-inaccessible) conformer. This is evident by the change in the dihedral angle χ_1 from 88.4° in apo-CheY to -174° in phosphono-CheY. In T87I CheY, the side-chain of Y106 is solvent-exposed (Figure 5), whereas in Y106W CheY the side-chain of W106 is solvent-inaccessible (*3*). In T87I/Y106W phosphono-CheY Trp106 remains in a g- solvent exposed position (Figure 6), forced out by the increased bulk of isoluecine 87 as described for T87I/Y106W CheY (*3*). In the phosphono-CheY structures presented here, the T87I mutation prevents the aromatic ring Y106 or W106 from rotating into the hydrophobic cavity between helix 4 and β-sheet 5 (Figures 4 and 5).

Discussion

E. coli CheY mutants T87I and T87I/Y106W CheY are able to accept a phosphoryl group on Asp57 at the active site but are unable to generate clockwise rotation of the flagella (*3*). In addition, both I87 mutants have ~5-fold lower autodephosphorylation rates and are completely resistant to CheZ activity (*36*). Thus, the presence of an isoleucyl side-chain at position 87 renders CheY phosphorylatable but unable to perform its chemotactic functions. Y106W CheY can also be phosphorylated, however, in contrast to I87 CheY mutants, Y106W CheY~P generates clockwise rotation above the level of wild-type CheY (*16*). Previous structural work was not carried out on the phosphorylated forms of these two mutants {Ganguli, 1995 #6}. In this study we attempt to determine whether the phosphorylated forms of these mutants are able to bind their protein partners and if not, to clarify the underlying structural reasons.

Eisenbach and collaborators demonstrated that the sixteen N-terminal residues of FliM compose the CheY-binding region of the flagellar switch protein (*33*). They also showed that a peptide with the sequence of the nineteen C-terminal residues of the phosphatase CheZ binds specifically to CheY~P, though at a lower affinity than that of intact CheZ (*37*). Both the FliM- and the CheZ-derived peptides bind more strongly to CheY~P than to CheY (*29*). We assume that these two peptides will reliably report the affinity that intact FliM and CheZ have for the three forms of phosphono-CheY studied here.

The FliM-derived peptide binds phosphono-CheY with slightly less affinity than its affinity for CheY~P. Qualitatively, the same is true for the CheZ-derived peptide (Table 2). These results imply that phosphono-CheY is a reasonable mimic of CheY~P; furthermore, we note that phosphono-CheY binds both full-length FliM and CheZ {Halkides, 1998 #66}. However, the FliM peptide shows no measurable affinity for either T87I phosphono-CheY or T87I/Y106W

phosphono-CheY. Similar results are obtained for the binding of the CheZ peptide to the various forms of CheY: The peptides bind only to phosphono-CheY, not to the two mutant forms of phosphono-CheY. These results indicate that the T87I mutation prevents binding to either peptide and that the Y106W mutation is unable to reinstitute binding ability.

We have generated crystal structures of T87I phosphono-CheY and T87I/Y106W phosphono-CheY to explain the results of our peptide binding studies and the known phenotypes of these mutants. Comparison of the structures of CheY and phosphono-CheY shows that the side-chain of Y106 moves from occupying both solvent-accessible and solvent-inaccessible conformations in the absence of the phosphoryl group at residue 57 to being exclusively solvent-inaccessible in its presence (*5*). In contrast, the aromatic ring of residue 106 is exclusively in the solvent-accessible conformation in the X-ray crystal structures of T87I CheY and T87I/Y106W CheY (*3, 15*), and unlike the wild-type protein phosphonomethylation does not alter its position (Figures 4 and 5). Evidently, the greater bulk of the side chain of the isoleucyl residue exacts too great a steric penalty to be overcome by any forces that tend to bring the aromatic side-chain of residue 106 into its solvent-inaccessible conformation.

A structure of BeF_3•CheY in complex with the FliM peptide displays a hydrophobic contact between the peptide and Y106, the side-chain of which adopts the solvent-inaccessible conformation (*12*). When the structure of this complex is superposed upon T87I phosphono-CheY, the FliM peptide clashes sterically with the aromatic side-chain of Y106, which must adopt the solvent-accessible conformation (data not shown). In further support the solvent-accessible conformation of W106 in D13K/Y106W CheY would also sterically clash with the FliM peptide (*38*). The structures of the complex between BeF_3•CheY and the CheZ peptide are similar to the complex between BeF_3•CheY and FliM, except that the CheZ peptide has *two*

binding modes to BeF_3•CheY, one of which is also observed in the BeF_3-free complex. In its solvent-inaccessible rotamer, the side-chain of Y106 interacts hydrophobically with the CheZ peptide in both modes, and both modes of binding are incompatible with Y106 in the solvent-accessible rotamer (*4*). These data are consistent with the proposition that the solvent-exposed conformation of residue 106 hinders or precludes the binding of CheY to peptides derived from FliM and CheZ.

Based on our peptide binding studies, the simplest explanation for the phenotypes of these two mutants is that T87I CheY~P and T87I/Y106W CheY~P fail to bring about clockwise rotation of flagella because they cannot bind FliM *in vivo*. With respect to chemotactic behavior, Matsumura and collaborators argued that binding between CheY and FliM is necessary but not sufficient for signaling (*16*). Other studies of residue 106 suggested that this residue does not alter the affinity of CheY~P for FliM but merely acts to propagate the signal after CheY~P·FliM association (*3*). For example, one possible post-binding role of residue 106 is to interact with Cδ of Ile95 (*38*). Our results do not exclude an additional role for residue 106.

Matsumura and collaborators observed an increase in resistance of T87I CheY~P and T87I/Y106W CheY~P to CheZ-promoted phosphatase activity (*36*). Furthermore, Bourret and collaborators reported that T87I CheY and T87C CheY display a decrease in CheZ-promoted dephosphorylation (*20*). Our results suggest that a lack of affinity of CheZ for CheY mutants T87I and T87I/Y106W is responsible for the observed increase in inertness toward CheZ-promoted hydrolysis. In analogy with the results on FliM, a decrease in binding affinity between the T87I mutants of CheY and CheZ is the simplest explanation for decreased CheZ-catalyzed phosphatase activity. However, we cannot exclude the possibility that the T87I mutation affects

CheZ-promoted hydrolysis in other ways, for example to reposition the Glu89 side-chain in a way that impairs catalysis (*39*).

In addition to the rotation of Y106, another aspect of CheY activation is a conformational shift of the 90's loop (*10*). In T87I/Y106W phosphono-CheY versus T87I/Y106W CheY, a shift of the 90's loop towards helix 3, the same direction of movement as beryllofluoride-activated CheY (*40*) versus apo-CheY (*7*) can be seen. This backbone change may be responding to a putative new hydrogen bond between Glu89 Oε and Lys91 Nε (see Results) and may have functional significance inasmuch as Glu89 participates in the CheZ-promoted hydrolysis of CheY~P (*39*). A larger change involving all residues of the loop and extending into helix 4 is observed when comparing T87I CheY with T87I phosphono-CheY. Overall the 90's loops of T87I and T87I/Y106W phosphono-CheY structures are similar to the loops in the beryllium-free complex (PDB accession no. 2fmf) and the loop in one of the BeF_3•CheY complexes (PDB accession no. 2fmh). The conformation of the loop in phosphono-CheY resembles the loop-up conformation observed for meta-active CheY (*11*).

Although residue 106 must remain in its solvent-accessible rotamer in the two phosphono-CheY mutants discussed here, this rotamer does not lock the 90's loop into a single conformation (Figure 2). One parameter that has been used to describe the loop is the pseudodihedral angle defined by the Cα atoms of residues 87 through 90 (*41*). Both T87I phosphono-CheY and T87I/Y106W have pseudodihedral angles that are similar to those seen in inactive conformations, and the values are slightly less than that for phosphono-CheY which has a pseudodihedral angle intermediate to that observed for BeF_3-activated CheY and apoCheY (Table 4). The values of ϕ and ψ for V86 are also similar to those observed for other inactive structures (Table 4). We acknowledge that the errors in dihedral and pseudodihedral angles

might be on the order of 20 degrees; however, small changes in protein structure are known to have large effects on function (*42*).

In conclusion, the structures of T87I phosphono-CheY and T87I/Y106W phosphono-CheY demonstrate that CheY mutants T87I and T87I/Y106W are unable to assume the active conformation upon phosphorylation. Additionally, the position of residue 106 in these CheY mutants is exclusively solvent-accessible. The results suggest that locking residue 106 in the "out position" precludes any structural rearrangements that lead to CheY activation and are consistent with the T-loop—Y model in which the solvent-accessible rotamer of Y106 specifies an inactive conformation of the loop (*41*). In addition to the lack of activation observed with T87I phosphono-CheY and T87I/Y106W phosphono-CheY, it appears that the solvent-accessible conformation of residue 106 would sterically interfere with FliM and CheZ binding. These observations offer an explanation for the phenotypes of *E. coli* mutants T87I CheY and T87I/Y106W CheY.

Acknowledgements

Use of the Advanced Photon Source was supported by U.S. Department of Energy, Basic Energy Sciences, Office of Science, under Contract No. W-31-109-Eng-38. Use of the BioCARS Sector 14 was supported by the National Institutes of Health, National Center for Research Resources, under grant number RR07707.

Supporting Information Available: δ-distance plots and C-alpha RMSD plots comparing T87I CheY with T87I phosphono-CheY and T87I/Y106W CheY with T87I/Y106W phosphono-CheY, as well as a δ-distance plot comparing the two solutions of T87I/Y106W phosphono-CheY are included as supplemental material. Refinement statistics for crystal 4 of T87I/Y106W phosphono-CheY are also included in the supplemental material. This material is available free of charge via the Internet at http://pubs.acs.org.

References

1. Matsumura, P., Rydel, J. J., Linzmeier, R., and Vacante, D. (1984) Overexpression and Sequence of the *Escherichia coli cheY* Gene and Biochemical Activities of the CheY Protein, *J. Bacteriol. 160*, 36-41.

2. Parkinson, J. S. (1993) Signal Transduction Schemes of Bacteria, *Cell 73*, 857-871.

3. Zhu, X., Rebello, J., Matsumura, P., and Volz, K. (1997a) Crystal Structures of CheY Mutants Y106W and T87I/Y106W: CheY Activation Correlates with Movement of Residue 106, *J. Biol. Chem. 272*, 5000-5006.

4. Guhaniyogi, J., Robinson, V., and Stock, A. (2006) Crystal Structures of Beryllium Fluoride-free and Beryllium Fluoride-bound CheY in Complex with the Conserved C-terminal Peptide of CheZ Reveal Dual Binding Modes Specific to CheY Conformation, *J. Mol. Biol. 359*, 624-645.

5. Halkides, C. J., McEvoy, M. M., Casper, E., Matsumura, P., Volz, K., and Dahlquist, F. W. (2000) The 1.9 Å Resolution Crystal Structure of Phosphono-CheY, an Analogue of the Active Form of the Response Regulator, CheY, *Biochemistry 39*, 5280-5286.

6. Stock, A. M., Mottonen, J. M., Stock, J. B., and Schutt, C. E. (1989) Three-dimensional structure of CheY, the response regulator of bacterial chemotaxis, *Nature 337*, 745-749.

7. Volz, K., and Matsumura, P. (1991) Crystal Structure of *Escherichia coli* CheY Refined at 1.7-Å Resolution, *J. Biol. Chem. 266*, 15511-15519.

8. Stock, A. M., Martinez-Hackert, E., Rasmussen, B. F., West, A. H., Stock, J. B., Ringe, D., and Petsko, G. A. (1993) Structure of the Mg^{2+}-Bound Form of CheY and Mechanism of Phosphoryl Transfer in Bacterial Chemotaxis, *Biochemistry 32*, 13375-13380.

9. Santoro, J., Bruix, M., Pascual, J., Lopez, E., Serrano, L., and Rico, M. (1995) Three-Dimensional Structure of Chemotactic CheY Protein in Aqueous Solution by Nuclear Magnetic Resonance Methods, *J. Mol. Biol. 247*, 717-725.

10. Lee, S.-Y., Cho, H. S., Pelton, J. G., Yan, D., Berry, E. A., and Wemmer, D. E. (2001) Crystal Structure of Activated CheY. Comparison With Other Activated Receiver Domains, *J. Biol. Chem. 276*, 16425-16431.

11. Simonovic, M., and Volz, K. (2001) A Distinct Meta-active Conformation in the 1.1-Å Resolution Structure of Wild-type ApoCheY, *J. Biol. Chem. 276*, 28637-28640.

12. Lee, S.-Y., Cho, H. S., Pelton, J. G., Yan, D., Henderson, R. K., King, D. S., Huang, L.-S., Kustu, S., Berry, E. A., and Wemmer, D. E. (2001) Crystal structure of an activated response regulator bound to its target, *Nat. Struct. Biol. 8*, 52-56.

13. Bourret, R. B., Drake, S. K., Chervitz, S. A., Simon, M. I., and Falke, J. J. (1993) Activation of the Phosphosignaling Protein CheY. II. Analysis of Activated Mutants by 19F NMR and Protein Engineering, *J. Biol. Chem. 268*, 13089-13096.

14. Lukat, G. S., Lee, B. H., Mottonen, J. M., Stock, A. M., and Stock, J. B. (1991) Roles of the Highly Conserved Aspartate and Lysine Residues in the Response Regulator of Bacterial Chemotaxis, *J. Biol. Chem. 266*, 8348-8354.

15. Ganguli, S., Wang, H., Matsumura, P., and Volz, K. (1995) Uncoupled Phosphorylation and Activation in Bacterial Chemotaxis. The 2.1-Å Structure of a Threonine to Isoleucine Mutant at Position 87 of CheY, *J. Biol. Chem. 270*, 17386-17393.

16. Zhu, X., Amsler, C. D., Volz, K., and Matsumura, P. (1996) Tyrosine 106 of CheY Plays an Important Role in Chemotaxis Signal Transduction in *Escherichia coli*, *J. Bacteriol. 178*, 4208-4215.

17. Sanders, D. A., Gillece-Castro, B. L., Stock, A. M., Burlingame, A. L., and Koshland, D. E., Jr. (1989) Identification of the Site of Phosphorylation of the Chemotaxis Response Regulator Protein, CheY, *J. Biol. Chem. 264*, 21770-21778.

18. Welch, M., Oosawa, K., Aizawa, S.-I., and Eisenbach, M. (1994) Effects of Phosphorylation, Mg^{2+}, and Conformation of the Chemotaxis Protein CheY on Its Binding to the Flagellar Switch Protein FliM, *Biochemistry 33*, 10470-10476.

19. Bourret, R. B., Hess, J. F., and Simon, M. I. (1990) Conserved aspartate residues and phosphorylation in signal transduction by the chemotaxis protein CheY, *Proc. Natl. Acad. Sci. U. S. A. 87*, 41-45.

20. Appleby, J. L., and Bourret, R. B. (1998) Proposed Signal Transduction Role for Conserved CheY Residue Thr87, a Member of the Response Regulator Active-Site Quintet, *J. Bacteriol. 180*, 3563-3569.

21. Volz, K. (1993) Structural Conservation in the CheY Superfamily, *Biochemistry 32*, 11741-11753.

22. Roman, S. J., Meyers, M., Volz, K., and Matsumura, P. (1992) A Chemotactic Signaling Surface on CheY Defined by Suppressors of Flagellar Switch Mutations, *J. Bacteriol. 174*, 6247-6255.

23. Halkides, C. J., Zhu, X., Phillion, D. P., Matsumura, P., and Dahlquist, F. W. (1998) Synthesis and Biochemical Characterization of an Analogue of CheY-Phosphate, a Signal Transduction Protein in Bacterial Chemotaxis, *Biochemistry 37*, 13674-13680.

24. Otwinowski, Z., Minor, W., and Charles W. Carter, Jr. (1997) Processing of X-ray Diffraction Data Collected in Oscillation Mode, *Methods Enzymol. 276*, 307-326.

25. Brünger, A. T., Adams, P. D., Clore, G. M., DeLano, W. L., Gros, P., Grosse-Kunstleve, R. W., Jiang, J.-S., Kuszewski, J., Nilges, M., Pannu, N. S., Read, R. J., Rice, L. M., Simonson, T., and Warren, G. L. (1998) Crystallography & NMR System: A New Software Suite for Macromolecular Structure Determination, *Acta Crystallogr., Sect. D: Biol. Crystallogr. 54*, 905-921.

26. Lovell, S. C., Davis, I. W., III, W. B. A., Bakker, P. I. W. d., Word, J. M., Prisant, M. G., Richardson, J. S., and Richardson, D. C. (2003) Structure validation by C-alpha geometry: phi, psi, and C-beta deviation, *Proteins: Struct., Funct., Genet. 50*, 437-450.

27. Laskowski, R. A., MacArthur, M. W., Moss, D. S., and Thornton, J. M. (1993) PROCHECK: a program to check the stereochemical quality of protein structures, *J. Appl. Crystallogr. 26*, 283-291.

28. Vriend, G. (1990) WHAT IF: A molecular modeling and drug design program, *J. Mol. Graphics 8*, 52-56.

29. McEvoy, M. M., Bren, A., Eisenbach, M., and Dahlquist, F. W. (1999) Identification of the Binding Interfaces on CheY for Two of its Targets, the Phosphatase CheZ and the Flagellar Switch Protein FliM., *J. Mol. Biol. 289*, 1423-1433.

30. Eftink, M. R. (1997) Fluorescence methods for studying equilibrium macromolecule-ligand interactions, *Methods Enzymol. 278*, 221-257.

31. Lowry, D. F., Roth, A. F., Rupert, P. B., Dahlquist, F. W., Moy, F. J., Domaille, P. J., and Matsumura, P. (1994) Signal Transduction in Chemotaxis, *J. Biol. Chem. 269*, 26358-26362.

32. Hess, J. F., Oosawa, K., Kaplan, N., and Simon, M. I. (1988) Phosphorylation of Three Proteins in the Signaling Pathway of Bacterial Chemotaxis, *Cell 53*, 79-87.

33. Bren, A., and Eisenbach, M. (1998) The N Terminus of the Flagellar Switch Protein, FliM, is the Binding Domain for the Chemotactic Response Regulator, CheY, *J. Mol. Biol. 278*, 507-514.

34. McEvoy, M. M., Hausrath, A. C., Randolph, G. B., Remington, S. J., and Dahlquist, F. W. (1998) Two binding modes reveal flexibility in kinase/response regulator interactions in the bacterial chemotaxis pathway, *Proc. Natl. Acad. Sci. U. S. A. 95*, 7333-7338.

35. Zhao, R., Collins, E. J., Bourret, R. B., and Silversmith, R. E. (2002) Structure and catalytic mechanism of the *E. coli* chemotaxis phosphatase CheZ, *Nat. Struct. Biol. 9*, 570-575.

36. Zhu, X., Volz, K., and Matsumura, P. (1997b) The CheZ-binding Surface of CheY Overlaps the CheA- and FliM-binding Surfaces, *J. Biol. Chem. 272*, 23758-23764.

37. Blat, Y., and Eisenbach, M. (1996) Conserved C-Terminus of the Phosphatase CheZ Is a Binding Domain for the Chemotactic Response Regulator CheY, *Biochemistry 35*, 5679-5683.

38. Dyer, C. M., Quillin, M. L., Campos, A., Lu, J., McEvoy, M. M., Hausrath, A. C., Westbrook, E. M., Matsumura, P., Matthews, B. W., and Dahlquist, F. M. (2004) Structure of the Constitutively Active Double Mutant CheY$^{D13K\ Y106W}$ Alone and in Complex with a FliM Peptide, *J. Mol. Biol. 342*, 1325-1335.

39. Silversmith, R. E., Guanga, G. P., Betts, L., Chu, C., Zhao, R., and Bourret, R. B. (2003) CheZ-Mediated Dephosphorylation of the *Escherichia coli* Chemotaxis Response Regulator CheY: Role for CheY Glutamate 89, *J. Bacteriol. 185*, 1495-1502.

40. Cho, H. S., Lee, S.-Y., Yan, D., Pan, X., Parkinson, J. S., Kustu, S., Wemmer, D. E., and Pelton, J. G. (2000) NMR Structure of Activated CheY, *J. Mol. Biol. 297*, 543-551.

41. Dyer, C. M., and Dahlquist, F. M. (2006) Switched or Not? The Structure of Unphosphorylated CheY Bound to the N-Terminus of FliM, *J. Bacteriol. in press*.

42. Mesecar, A. D., Stoddard, B. L., and Koshland, D. E., Jr. (1997) Orbital Steering in the Catalytic Power of Enzymes: Small Structural Changes with Large Catalytic Consequences, *Science 277*, 202-206.

Table 1: Data Collection and Refinement Summary

	T87I Phosphono-CheY	T87I/Y106W Phosphono CheY
Space group	$P2_12_12_1$	$P2_12_12_1$
Unit cell dimensions a, b, c	41.35, 49.96, 53.90	40.06, 50.18, 53.13
Refinement resolution (Å)	20.0 – 1.75	20.0 – 1.85
Total theoretical no. of reflections	11733	9574
Tot. no. collected	99128	91397
No. reflections used	10988	8281
Reflections work/test	10419/569	7863/418
I/σ	22.1 (4.6)	15.2 (1.0)
Completeness (%)	95.0 (57.3)	86.1 (75.2)
R(sym)	0.047 (0.15)	0.083 (0.99)
χ^2	0.93 (1.23)	1.93 (1.88)
No. of molecules in AU	1	1
No. residues	128 (6 disordered)	128 (7 dis.)
No. protein atoms	1033	1045
No. solvent atoms	116	79
No. acetate atoms	0	0
R_{free}	0.199	0.312
R_{cryst}	0.167	0.242
FOM	0.905	0.676
RMSD bond lengths (Å)	0.018	0.015
RMSD bond angles (degrees)	1.5	1.4

Table 2: Dissociation constants of peptides from CheY

Protein	K_d, FliM peptide, µM	K_d, CheZ peptide, µM
CheY	680 ± 10 [a]	440 ± 10[a]
CheY-P_i	27 ± 1 [a]	26 ± 1[a]
Phosphono-CheY	38 ± 1	58 ± 4
T87I Phosphono-CheY	Not detectable	Not detectable
T87I/Y106W Phosphono-CheY	Not detectable	Not Detectable

[a] McEvoy et al., (1999) *J. Mol.Biol. 289,* 1423-1433.

Table 3: Distances (in Å) between phosphoryl-group oxygen atoms and selected nitrogen atoms

Residue	Phosphono-CheY[a]	T87I phosphono-CheY Pcy57 A	T87I phosphono-CheY Pcy57 B	T87I/Y106W phosphono-CheY
Asn59 NH	5.50	4.02	2.70	3.31
Ala88 NH	3.73	3.71	3.45	3.16
Trp58 NH	5.98	4.47	3.54	3.71
Lys109 Nε	2.95	2.79	3.69	3.38

[a]Halkides *et al*., (2000) *Biochemistry 39,* 5280-5286.

Table 4: Pseudodihedral angles of residues 87-90 and main-chain dihedral angles of Val86

Protein	87-90 Cα Pseudodihedral Angle	Val86 ϕ	Val86 ψ
T87I CheY[a]	21	-103	123
T87I phosphono-CheY	22	-112	123
T87I/Y106W CheY[b]	13	-93	109
T87I/Y106W phosphono-CheY	16	-99	123
Phosphono-CheY[c]	44	-117	133

[a]Ganguli *et al.,* (1995) *J. Biol. Chem 270,* 17386-17393.
[b]Zhu *et al.,* (1997) *J. Biol. Chem 272,* 5000-5006.
[c]Halkides *et al.*, (2000) *Biochemistry 39,* 5280-5286.

Figure Legends

Figure 1: Schematic representation of the active site of phosphono-CheY. Side-chains are shown terminating in Cα atoms. Protonation states are inferred.

Figure 2: The 90's loop of T87I CheY (yellow), T87I/Y106W CheY (green), T87I phosphono-CheY (cyan), and T87I/Y106W phosphono-CheY (orange). In both mutants, phosphonomethylation results in a shift of the loop away from the α_4-β_5-α_5 signaling surface.

Figure 3: Active site of T87I phosphono-CheY showing both conformations of the phosphonomethyl group, Pcy57 A and Pcy57 B. Also shown are the hydrogen bonds from Lys109 to the phosphoryl oxygens of Pcy57 A and from Asn59 to the phosphoryl oxygens of Pcy57 B.

Figure 4: Active site of T87I/Y106W phosphono-CheY (crystal 3) compared to Phosphono-CheY. The phosphoryl group of T87I/Y106W phosphono-CheY is closer to the amide bonds of Trp58 and Asn59.

Figure 5: Position of Y106 in T87I phosphono-CheY (white) and T87I CheY (grey). In both structures the aromatic ring is observed in its solvent-accessible rotamer.

Figure 6: Position of W106 in T87I/Y106W phosphono-CheY (white) and Y106W CheY (grey). In Y106W CheY the aromatic side-chain is in its solvent-inaccessible rotamer, whereas in T87I/Y106 W CheY it is solvent accessible. Only the solvent-inaccessible rotamer is compatible with binding peptides derived from FliM or CheZ.

Figure 1

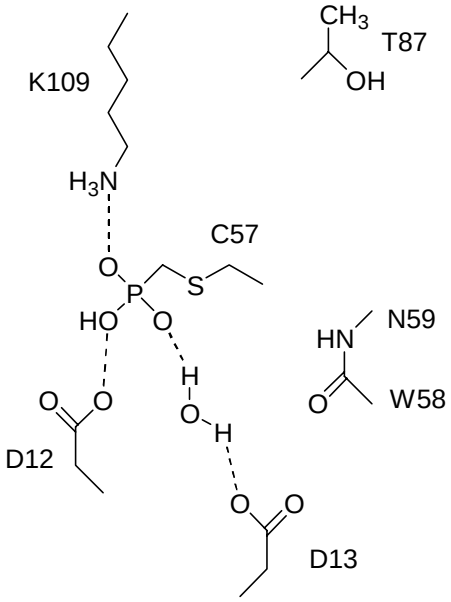

Figure 2

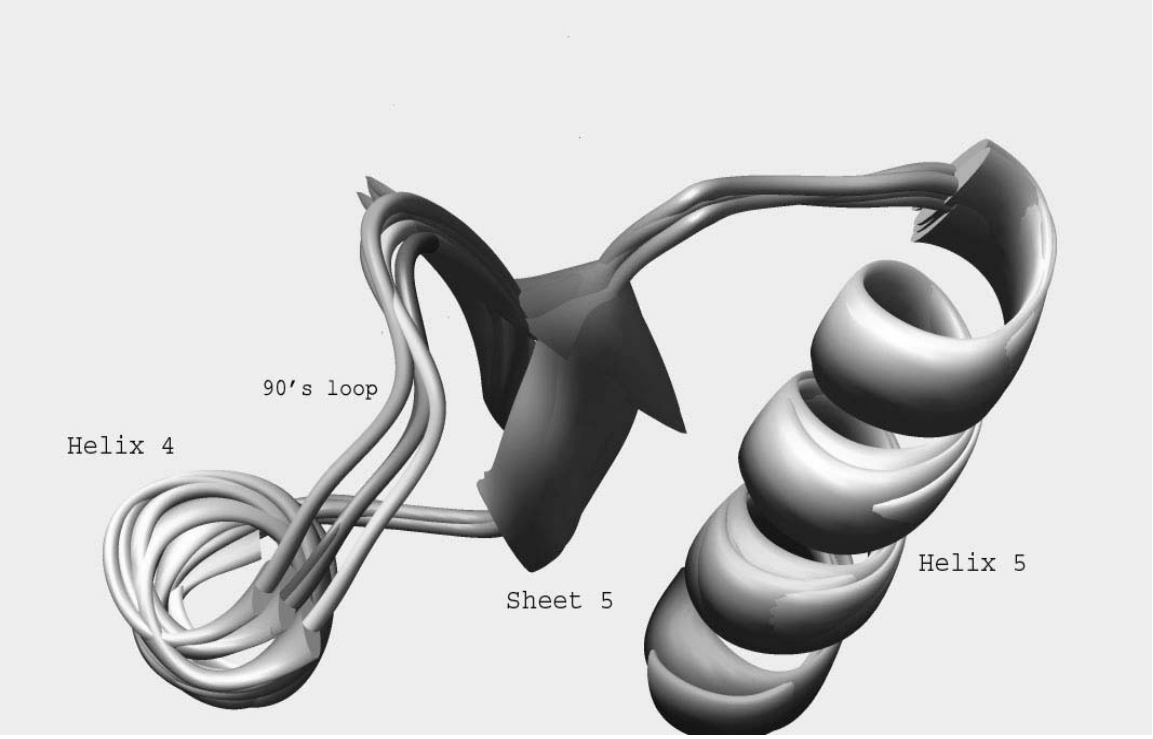

Figure 3

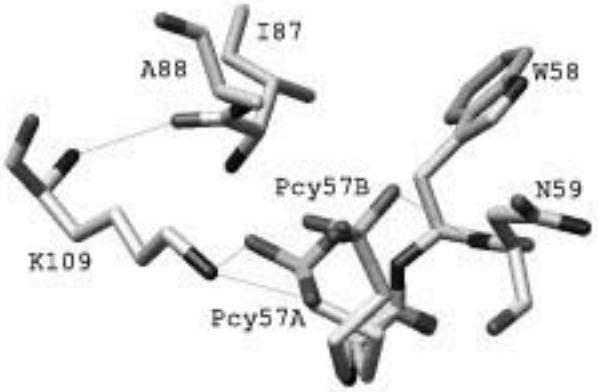

Figure 4

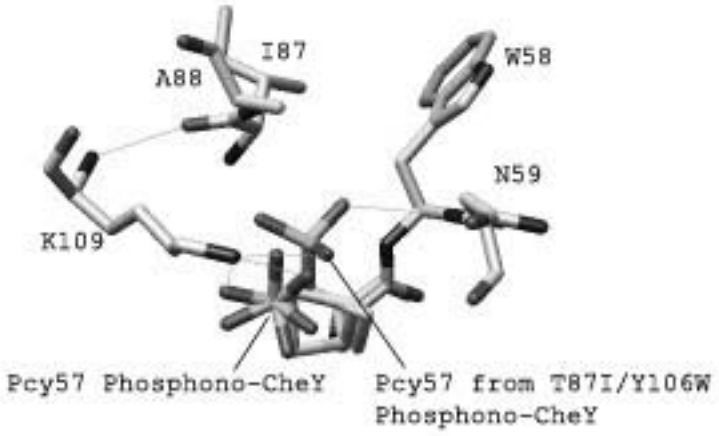
I87
A88
W58
N59
K109
Pcy57 Phosphono-CheY
Pcy57 from T87I/Y106W
Phosphono-CheY

Figure 5

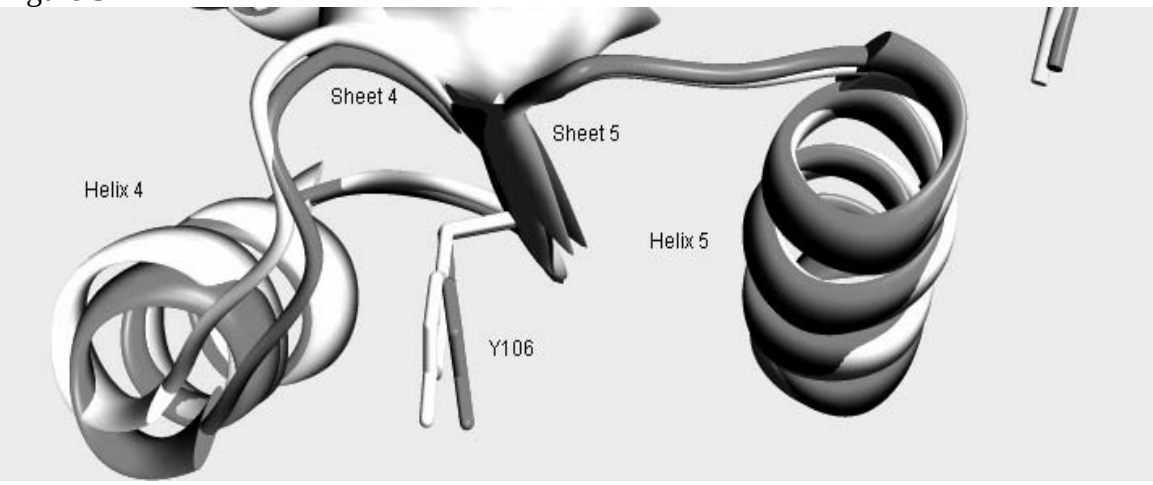

Figure 6

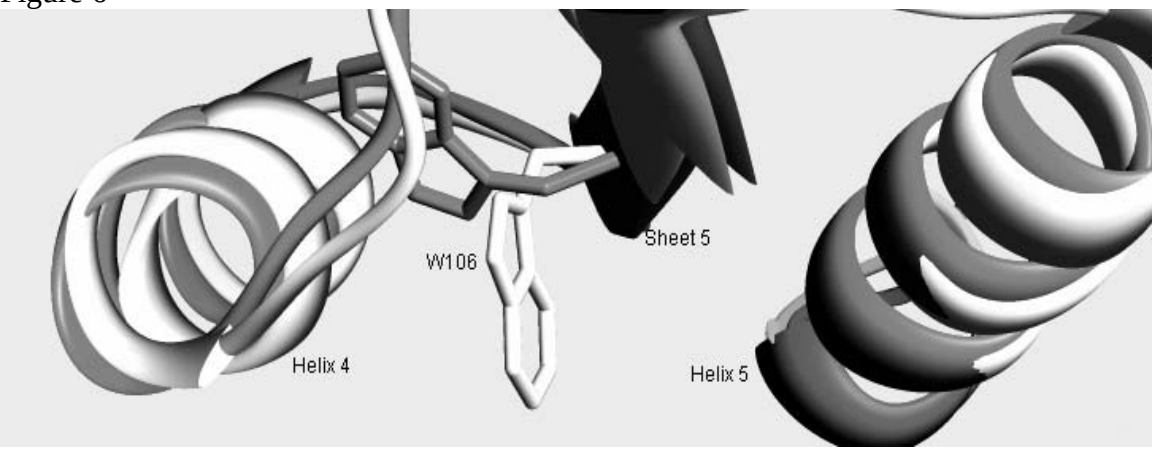

TOC Graphic